Journal of Thermal Analysis and Calorimetry
https://doi.org/10.1007/s10973-020-09659-y

Surface tension of supercooled graphene oxide nanofluids measured with acoustic levitation

Yudong Liu[1,2] · Bing Chen[1,2] · Dengshi Wang[3] · Nan Jiang[3] · Junkun Tan[1,2] · Jing Fu[1,2] · Baohui Wu[1,2] · Yuanhao Hu[1,2] · Zhihong Guo[1,2]

Received: 11 January 2020 / Accepted: 31 March 2020
© Akadémiai Kiadó, Budapest, Hungary 2020

Abstract

The surface tensions of graphene oxide nanofluids of five mass concentrations were measured by the oscillation droplet method in an acoustic levitator. The oscillation information of the suspension droplets was obtained by combining acoustic levitation with image recognition technology, and a shape correction coefficient a was introduced to modify the Rayleigh equation. Over the temperature ranging from − 7 to 10 °C, the surface tension of the graphene oxide nanofluids increases with increasing mass concentration and decreases with increasing temperature. Compared with the surface tension changes caused by an increase in the mass concentrations of nanofluids from 0.08 to 0.12% at − 7 °C, the surface tension slowly increases from 79.144 to 80.664 mN m^{-1} when the mass concentration increases from 0.02 to 0.08%. The change rate of the surface tension with temperature is linear in both supercooled and non-supercooled states. For nanofluids with a mass concentration of 0.02%, the values are − 0.185 and − 0.186, respectively, which are basically the same. However, with an increase in mass concentration, the surface tension increases abnormally in supercooled state. For nanofluids with mass concentrations of 0.05% and 0.08%, the curve of the surface tension has an inflection point at − 1.0 °C, while for mass concentrations of 0.10% and 0.12%, the inflection point is at 1.0 °C. All inflection points are distributed around the triple point temperature of water.

Keywords Nanofluids · Surface tension · Supercooled · Acoustic levitation

List of symbols

A	Amplitude
a	Correction coefficient
B	The constant term of the Rayleigh equation
f_R, f	The natural oscillation frequency and oscillation frequency of the droplet, respectively (Hz)
l	The oscillating mode of liquid suspension droplet
M	The mass of the droplet (kg)
T, T_C	Absolute temperature and critical temperature, respectively (K)
x	Time (s)
y, y_0	The length of droplet's long axis and the average length, respectively
δ, $\bar{\delta}$	Surface tension and average surface tension (mN m^{-1})
ω	Angular velocity (rad s^{-1})
φ	Initial phase (rad)

Subscript

C	Critical state
R	Rayleigh equation
0	Original state

Introduction

Nanofluids refer to the dilute suspensions prepared by the dispersion of metallic or nonmetallic nanoparticles, with a typical size of less than 100 nm, in base fluids. Since first being utilized by Choi [1], nanofluids have attracted extensive attention due to their good thermal conductivity [2–5] and phase change characteristics [6–8]. For a further understanding of nanofluids, it is necessary to accurately measure their thermophysical properties. The surface tension of nanofluids plays a vital role in mass transfer [9, 10], droplet deformation [11–13], solid/liquid interface wettability [14],

✉ Yudong Liu
ydliu2000@163.com

[1] School of Energy and Power Engineering, Chongqing University, Chongqing 400044, China

[2] Chongqing University Key Laboratory of Low-Grade Energy Utilization Technologies and Systems of Ministry of Education, Chongqing 400044, China

[3] Chongqing Institute of Graphene, Chongqing 404100, China

Published online: 11 April 2020

and the interface phenomenon during fluid flow [15, 16]. As we know, the carbon structures nanomaterials have better performance than the traditional metal, so the surface tension of carbon structures nanofluids have great potential to be studied. Therefore, it is extremely important to measure surface tension of carbon structures nanofluids.

In addition, a brief review of recent studied on surface tension of carbon structures nanofluids can expand understandings the evolution of the surface tension. For instance, several researchers reported the surface tension of graphene oxide nanofluids with different mass concentrations at temperature (10–100 °C). An enhancement of 2.9% in surface tension has been observed at the maximum mass concentration (0.10%). It has been found that the surface tension increased with the graphene oxide nanoparticles concentration [17]. Kamatchi et al. [18] investigated the effect of the nanoparticles concentrations (0.01–0.03 mass%) and temperature (35–75 °C) on the surface tension of reduced graphene oxide nanofluids. The result showed that the surface tension of the nanofluids is higher than that of water and increases with concentrations. Moreover, Ahammed et al. [19] examined the surface tension of graphene nanofluids with volume concentration and temperature. When the volume concentration was maintained at 0.15%, the surface tension of nanofluid in the temperature measurement range decreased by 18.7% compared with that of deionized water. It should be noted that the surface tension of graphene nanofluids decreased with the increase in the both concentration and temperature. Furthermore, Cabaleiro et al. [20] studied the surface tension of graphene oxide at ambient temperature. They believed that diminutions in surface tension can be attributed to the increase in the intermolecular spacing at the liquid–air interface, which can reduce the attractive force between water molecules that are inside the droplet.

Besides graphene nanofluids, some researchers have studied the surface tension of carbon nanotubes nanofluids with concentrations (0.1–10 mass%). The surface tension of multi-walled carbon nanotubes nanofluids with 10 mass% enhanced by 7% compared to that of deionized water. It has been found that the surface tension initially decreased with concentration and then increases [21]. Karthikeyan et al. [22] experimentally measured the surface tension of functionalized multi-walled carbon nanotubes nanofluids with volume concentration (0.001–0.012%). It has been observed that the surface tension of nanofluids did slightly change, only when the concentration of nanofluids exceeds the critical concentration, the surface tension of the nanofluid increases linearly with the concentration. Moreover, Berrada et al. [23] noted that the surface tension evolution was intensively depended on the surface properties of carbon nanomaterials, and the hydrophobic functional groups on the surface of carbon nanotube generated the surface tension reduction with nanofluid concentration. Furthermore, Karami et al. [24] reported the surface tension of functionalized graphene and multi-walled carbon nanotubes nanofluids with various concentrations. The results showed that the surface tension of nanofluids decreased with the increase in nanoparticle concentrations.

The above researchers must contact a solid material with the tested fluid sample during the surface tension measurement of nanofluids. Therefore, during the test, one must carefully clean the experimental hardware and prevent contamination of the sample from the containers. Furthermore, due to the wetting conditions, various solid materials may be used for different fluids, and much effort is required for calibration of the measurement system. Acoustic levitation provides a containerless technology to measure the surface tension of fluids. During the process of measurement, a small test droplet is levitated and isolated within another medium by the acoustic radiation stress on the droplet's surface. Usually, the levitated droplet is excited into shape oscillations, and the surface tension is obtained by measuring the oscillation frequency accordingly. Acoustic levitation has no special requirements for the levitated droplet, so it is widely used in research on the solidification of materials [25], biomedicine [26, 27], and droplet dynamics [28–30].

For most commonly used fluids, such as water and various mixed liquids, surface tension has been relatively well tested. Nevertheless, the available experimental data are still scarce in some temperature regions. Moreover, most of the surface tension data are limited to stable thermodynamic conditions. In this paper, we focus on the surface tension of graphene oxide nanofluids in supercooled state, i.e., when the supercooled nanofluids are cooled below freezing, which is a metastable state. The surface tension of the supercooled nanofluids plays an important role in the nucleation of nanofluids. It is very difficult to measure the surface tension in supercooled region, which is the temperature zone of nucleation. In this paper, we utilize acoustic levitation combined with image recognition to measure the surface tension of the supercooled graphene oxide nanofluids by detecting the oscillation information of the levitated graphene oxide nanofluid droplets.

Experimental

Surface tension measuring apparatus

Figure 1 shows the schematic of the surface tension measuring apparatus. This device consists of an acoustic levitator, a thermostatic bath, and a data acquisition system. A high-intensity ultrasonic wave is generated by an ultrasonic transducer driven at a resonant frequency of 20 kHz. A vertical titanium alloy ultrasonic horn is attached axially to the ultrasonic transducer. The ultrasonic wave radiates from the

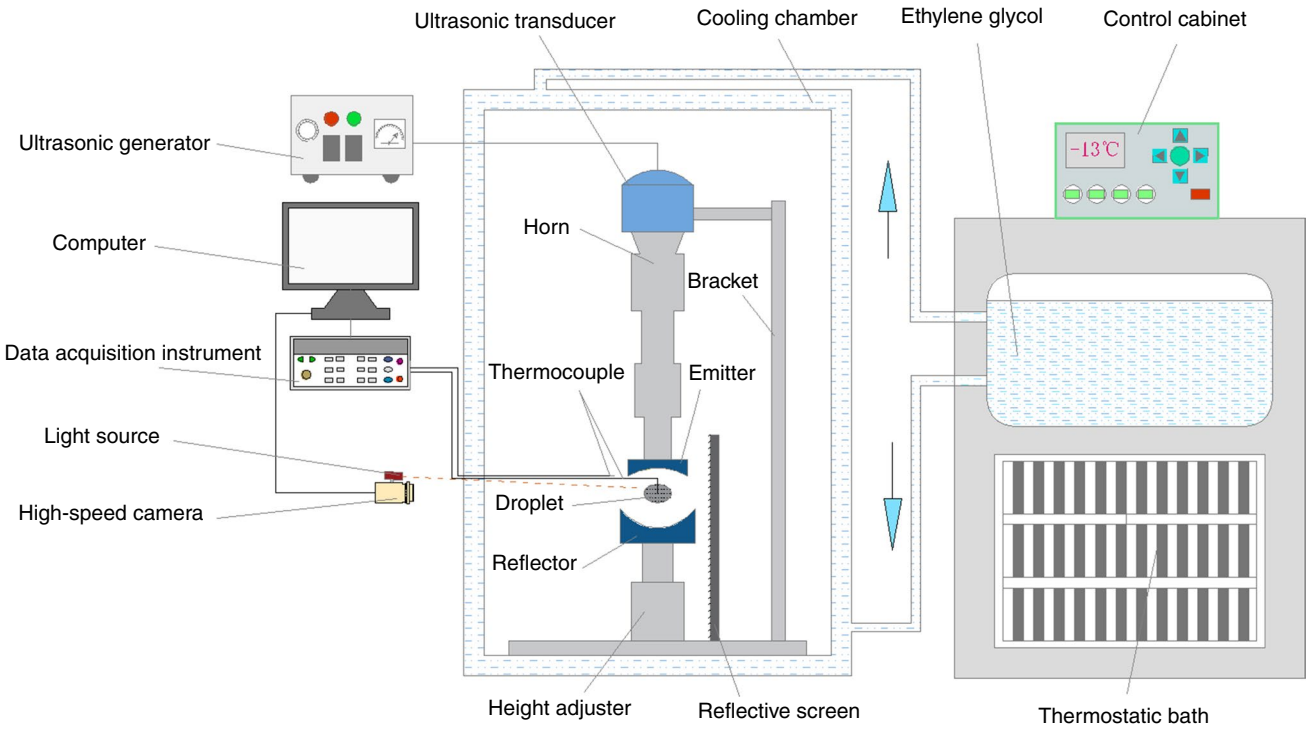

Fig. 1 Schematic of the surface tension measuring apparatus

emitter and is reflected by a concave reflector whose distance from the emitter is adjusted via a height adjuster. When the ultrasonic horn and the reflector are separated by an appropriate distance, a standing wave is formed in the gap. The acoustic pressure varies as the square of a sine wave along the horn–reflector axis. The concavity of the reflector serves to radially focus the acoustic pressure into points where a droplet of nanofluid may be stably levitated against gravity.

The temperature inside the cooling chamber is controlled by setting the temperature of the ethylene glycol solution, which flows recurrently between the cooling chamber and the thermostatic bath. The lowest temperature of the ethylene glycol solution can be set at − 15 °C during experiments. Considering the large measurement inaccuracy of infrared thermometers at low temperatures, copper–constantan (T-type) thermocouples are used to measure the temperature of both the air inside the cooling chamber and the levitated droplet. These temperatures were recorded by a data acquisition instrument (Agilent 34970A). The precision of the thermocouples is ± 0.2 °C, as calibrated by a high precision thermometer.

When the temperature inside the cooling chamber is stable, the distance between the emitter and the reflector should be carefully adjusted to reach a resonance state. Then, a 40 μL droplet is manually injected to the node of the standing wave through a small window by a pipette to make it levitate stably by adjusting the power of the ultrasonic generator. The thermocouple preset at the node of the standing wave is accordingly moved to the center position of the droplet, and when the temperature of the droplet reaches a stable value, the droplet is slightly disturbed by blowing air on it with a syringe in order to generate oscillation [31]. At the same time, a high-speed camera (Basler acA2040-90uc) is utilized to continuously record the images of the levitated droplet at a rate of 800 fps. Repetitive experiments were carried out six times at each temperature in order to ensure the reliability of the experimental data.

Preparation and characterization of graphene oxide nanofluids

The graphene oxide nanofluids were prepared by the two-step method. The graphene oxide nanomaterial (longest diameter: 500 nm–5 μm, a single-layer ratio of 99%, thickness: 0.8–1.2 nm) was purchased from XFNANO company (china). The graphene oxide nanomaterial was evenly dispersed in deionized water (resistivity: 18 MΩ cm at 20 °C) by an ultrasonic stirrer (FS-300, supplied by SONXI company in china). The power of the ultrasonic oscillator was set at 300 W with 8 s pulse mode for 150 min. Figure 2 shows that the mass concentrations of the graphene oxide nanofluids are 0.02%, 0.05%, 0.08%, 0.10%, and 0.12%, respectively.

Fig. 2 Image of the graphene oxide nanofluid with different mass concentrations

Table 1 Particle size and Zeta potential distribution of the different mass concentrations of graphene oxide nanofluids

Graphene oxide nanofluids/mass%	Particle size (over 90%)/nm	Average particle size/nm	Zeta potential (absolute)/mV	Average Zeta potential/mV
0.02	73–165	98	0–51	30
0.05	20–45	30	0–75	42
0.08	15–50	37	0–86	47

The particle size distribution and Zeta potential of the graphene oxide nanofluids are measured by a laser size and zeta potential analyzer (Nano ZS90). Table 1 shows the distribution of the particle size and zeta potential of the graphene oxide nanofluids with three mass concentrations. The zeta potential of the graphene oxide nanofluids with different mass concentrations is greater than the critical stable value (the absolute value is 30 mV) [32], which indicates that the graphene oxide nanofluids possess excellent stability.

Droplet oscillation and image recognition

Principle of measuring surface tension by the oscillating droplet method

For a near spherical inviscid liquid drop, the frequency of oscillation is expressed by the Rayleigh equation [33],

$$\delta = \frac{3}{l(l-1)(l+2)}\pi M f_{\mathrm{R}}^2 \tag{1}$$

where δ, f_{R} are the surface tension and natural frequency of the droplet, respectively. M is the mass of the suspended droplet, which can be determined by a volume reading of the pipette. The precision of the pipette is ± 1 mg, as calibrated by a high-precision electronic balance. L is the resonant mode, which can be observed by oscillating the droplet. The surface tension is proportional to the square of the natural frequency f_{R}. This suggests the method for measuring the surface tension via the frequency of an oscillating droplet.

Before measuring the frequency, it necessary to judge the droplet resonant mode l. A binary image composed of black and white pixels is obtained by processing the recorded image during the process of droplet oscillation, and the area of the black pixels represents the droplet. Figure 3 shows a binary image of the 0.05 mass% graphene oxide nanofluid droplets at -5.0 °C in an oscillation period. Alternating flattening and extension of poles of the droplets, consistent with the oblate–prolate oscillation of the fundamental ($l=2$) mode, can be seen in this figure. By observing the oscillation process of the droplets at different measurement temperatures, the resonant mode of the droplets is determined to be $l=2$.

Indeed, the initial shape of the suspended droplets is non-spherical according to the balance among the surface tension, the gravity, and the acoustic radiation pressure. The Rayleigh equation is modified by introducing the correction coefficient a [34–36], which is determined by fitting the measurement data.

$$\delta = \frac{3}{8}a\pi M f^2 \tag{2}$$

Processing the suspension droplet images

In order to obtain the oscillation frequency of the droplet, the image recognition software ImageJ combined with

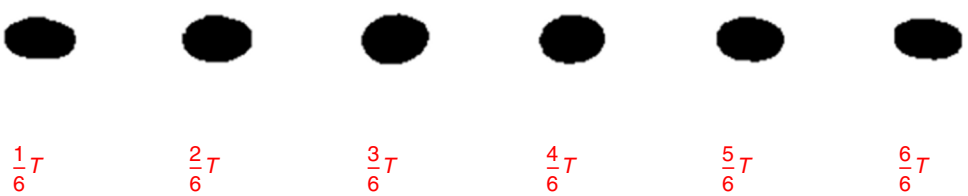

Fig. 3 Binary image of a periodic oscillation of 0.05 mass% nanofluid droplets at -5 °C

self-programming which is used to batch process images of the collected droplet. Figure 4 shows the image processing flow of the acoustic suspension nanofluid droplet at $t = \frac{3}{6}T$ in Fig. 3. First, the original RGB image of the droplet is converted into a grayscale image. To retain the droplet's shape information, the software can significantly remove interference signals and reduce the computational complexity of the boundary recognition. Then, by subtracting the background image, the interference of the thermocouples, the shadow of the thermocouple, and the shadow below the droplet are eliminated. Finally, the Canny [37] method is used to generate the boundary of the droplets, and after the dilation, erosion, and filling operations, the shape of the droplet is elliptically fitted to obtain the data of the long axis, short axis, and centroid.

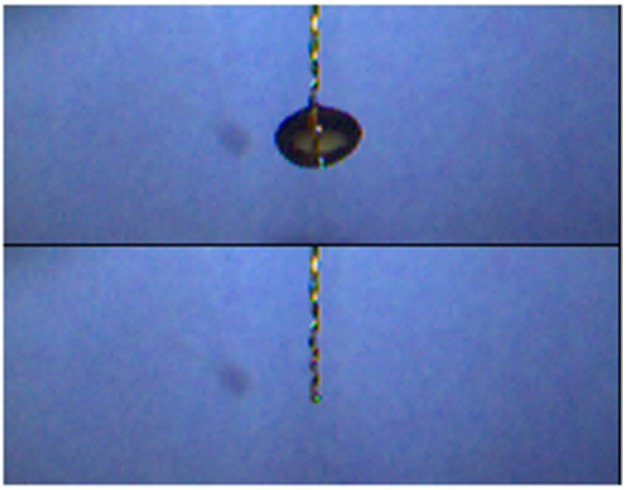

(a) RGB image of the droplet and background

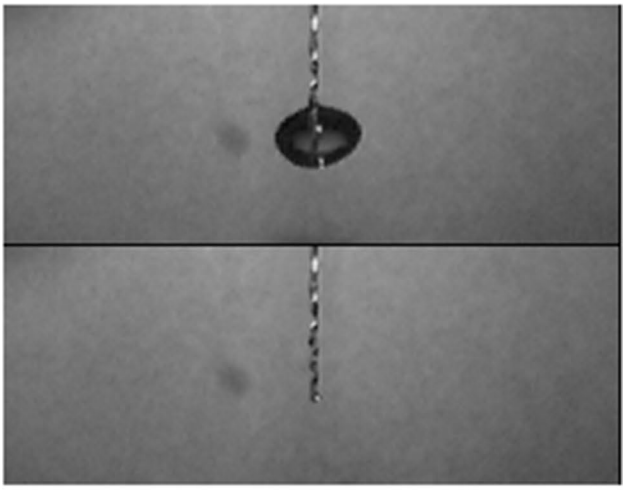

(b) Image after grayscale conversion

(c) Binary image of the droplet after processing

(d) Image of the droplet after ellipse fitting

Fig. 4 Image processing flow of the 0.05 mass% nanofluid droplets at − 5.0 °C

For nanofluid with mass concentration of 0.05% at − 5.0 °C, the long axis changes of an oscillation droplet over a period of time are shown in Fig. 5. This value varies in a sinusoidal manner and can be fitted by $y(x) = y_0(1 + A\sin(\omega x + \varphi))$ with $y_0 = 23.986$ pixels, $A = 0.127$, $\omega = 90.2\pi$, $\varphi = 43.382\pi$. This means that the drop oscillates at a frequency of 45.1 Hz. Besides fitting the droplet data to obtain the oscillation frequency, it can also use the fast Fourier transform (FFT) to analyze the droplet data, as shown in Fig. 6. The dominant frequency in the spectrum diagram represents the oscillation frequency f of the suspension droplet.

Meanwhile, it is observed that there is a second peak in the spectrum diagram, the corresponding frequency is 50 Hz, which is the same as the input current frequency of the ultrasonic generator in the acoustic levitation system. The principle of the ultrasonic generator is to convert the 50 Hz AC in the power grid into the required high frequency through the circuit module. However, the output signal of ultrasonic generator is mixed with the unconverted low-frequency signal and this low-frequency signal through the ultrasonic transducer and ultrasonic horn to the suspended droplets, which causes that the droplet appears a small vibration with a frequency of 50 Hz. As a result, a second peak (50 Hz) appears in the spectrum diagram. In addition, the amplitude of the

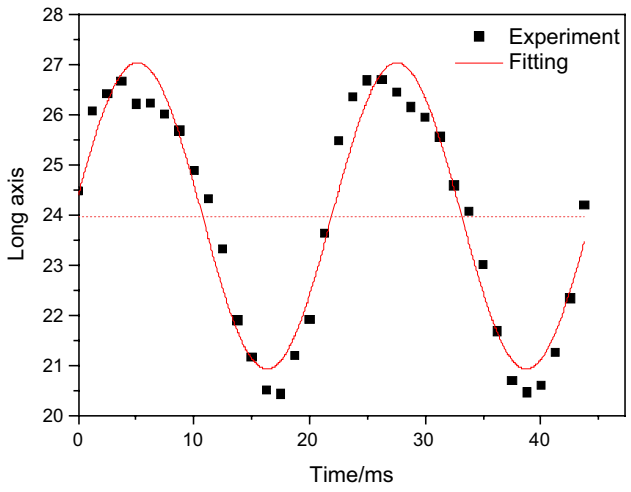

Fig. 5 Curve of the time evolution of the long axis of the 0.05 mass% nanofluid droplets at − 5.0 °C

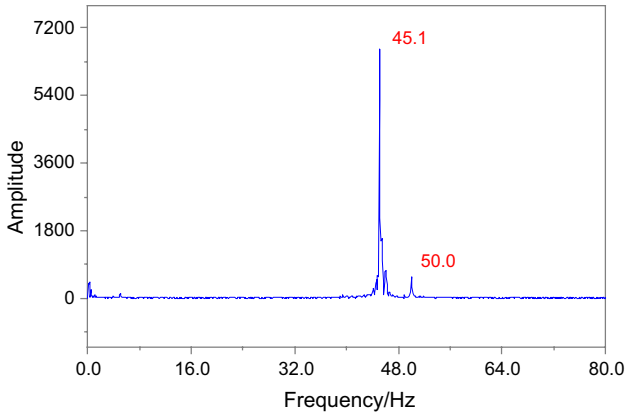

Fig. 6 Spectrum of 0.05 mass% nanofluid droplets oscillation at − 5.0 °C

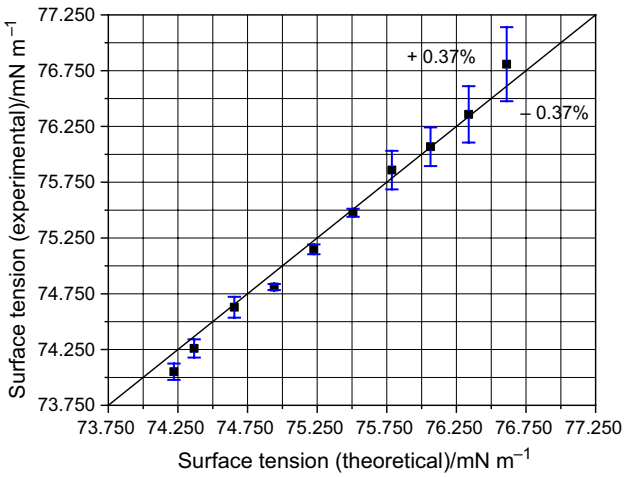

Fig. 7 Surface tension of experimental and theoretical results for deionized water

second peak is only 8.66% of the amplitude of the main peak, so the interference of the second peak on the result can be ignored.

Results and discussion

Verification the surface tension of deionized water

In order to verify the feasibility of the method, the surface tension of deionized water in the range from − 7.0 to 10.0 °C was measured. The experiment was repeated six times for each temperature to calculate the average of the experimental data, and the deviations from the mean value are within ± 0.43%. The theoretical data of surface tension can be determined by the Vargaftik equation [38].

$$\delta = B\left(1-\frac{T}{T_C}\right)^{1.256}\left(1-0.625\left(1-\frac{T}{T_C}\right)\right) \tag{3}$$

where T is the absolute temperature (K), T_C is the critical temperature of water, and $B = 235.8$ mN m^{-1}.

The surface tension of deionized water at 10.0 °C is taken as the datum, and the oscillation frequency f of the suspended water droplets at 10.0 °C was put into the Eq. (2), to determine the correction coefficient of deionized water $a = 0.784$. Figure 7 shows the result of the measurements in this paper and theoretical data. The measured values agree well with theoretical data, and the average deviation is ± 0.37%. This is enough to prove that the surface tension measurement method adopted in this paper can accurately and effectively measure the surface tension of droplets and is suitable for supercooled fluids.

Determination of the correction coefficient *a*

Based on Eq. (2), in order to determine the surface tension of the graphene oxide nanofluids in supercooled state, in addition to measuring the oscillation frequency f of the suspended droplets, it is also necessary to determine the correction coefficient a that corresponds to different mass concentrations of nanofluids. In this paper, the surface tension of the graphene oxide nanofluids at 10.0 °C is taken as the benchmark, which is obtained by using the method of Zheng [17] (the ring method). Figure 8 shows that the oscillation frequency spectra of the graphene oxide nanofluid droplets with five mass concentrations processed by FFT at the base temperature. In this way, the corresponding oscillation frequency f is obtained. Table 2 shows the correction coefficient a, determined by combining Eq. (1) with Eq. (2), where $\overline{\delta}$ is the average of six repeated tests.

Effect of mass concentrations on surface tension

Figure 9 shows the surface tension of the graphene oxide nanofluids with different mass concentrations at − 7.0 °C. According to the measured results, with an increase in mass concentration, the surface tension of the nanofluids increases at the same temperature. This likely occurs because hydrophilic graphene oxide nanoparticles are added to the water, and these nanoparticles are more distributed in the interior of droplets, while the attraction between the nanoparticles and water molecules is stronger than that between the water molecules, which makes the water molecules on the surface of the droplets flow inward, resulting in a decrease in the molecule spacing at the interface of the droplets and increases surface tension. Moreover, there are fewer nanoparticles on the surface of droplets. This will further reduce

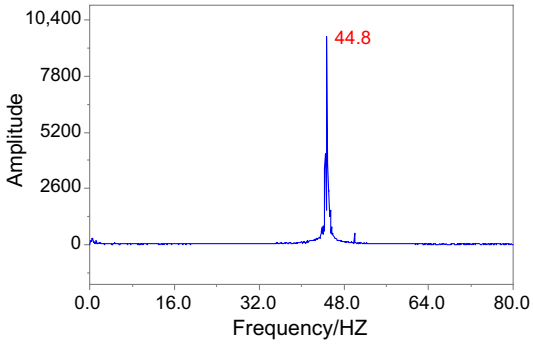

(a) Spectrum of 0.02 mass% graphene oxide nanofluid droplet oscillation

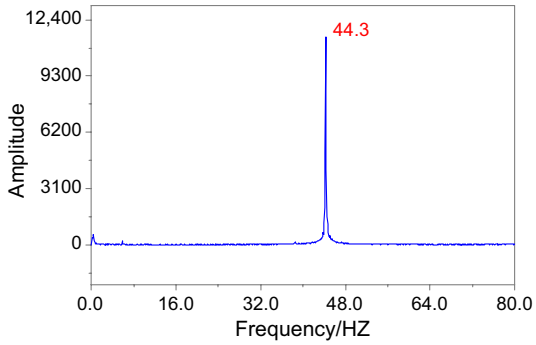

(b) Spectrum of 0.05 mass% graphene oxide nanofluid droplet oscillation

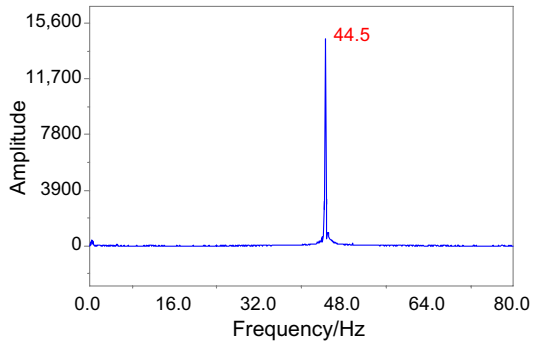

(c) Spectrum of 0.08 mass% graphene oxide nanofluid droplet oscillation

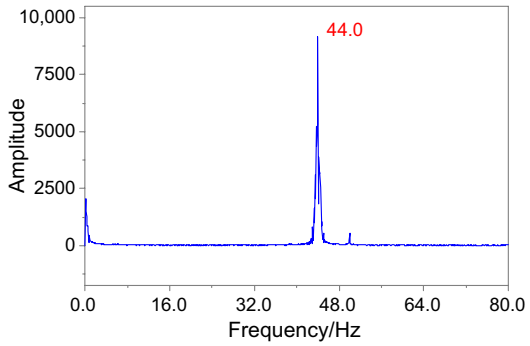

(d) Spectrum of 0.10 mass% graphene oxide nanofluid droplet oscillation

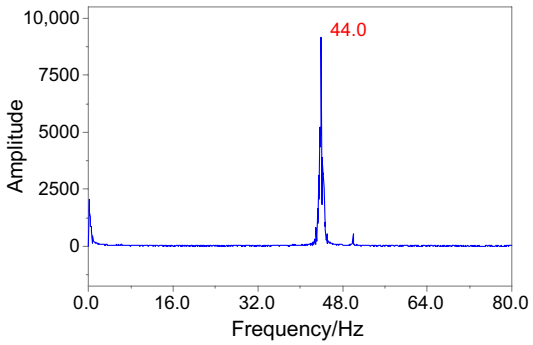

(e) Spectrum of 0.12 mass% graphene oxide nanofluid droplet oscillation

Fig. 8 Spectrum of droplet oscillation at the reference temperatures

Table 2 Correction coefficient a of graphene oxide nanofluids at the reference temperature

Graphene oxide nanofluids/mass%	Temperature/°C	Reference value [17]/mN m^{-1}	$\bar{\delta}$/mN m^{-1}	a
0.02	10.0	76.000	94.842	0.801
0.05	10.0	76.600	92.588	0.827
0.08	10.0	77.530	93.447	0.829
0.10	10.0	77.300	92.383	0.836
0.12	10.0	77.020	91.282	0.843

the molecule's space under strong interactions with water molecules. In addition, some researchers [39, 40] have shown that nanoparticles with specific functional groups will be charged in the base liquid, and these charged nanoparticles will be enriched and assembled at the gas/liquid interface, which may also lead to changes in the surface tension of the nanofluids.

Moreover, the experimental results clearly show that when the mass concentration is lower than 0.08%, the change rate of the surface tension with mass concentration is smaller than that of a higher mass concentration, and the surface

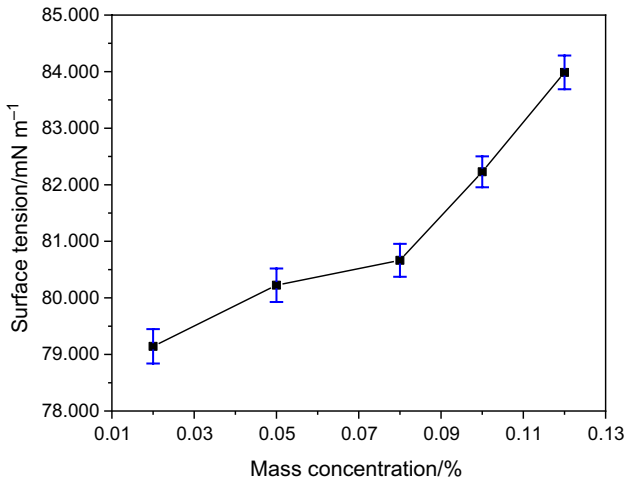

Fig. 9 Surface tension of the graphene oxide nanofluid varies with mass concentration at − 7.0 °C

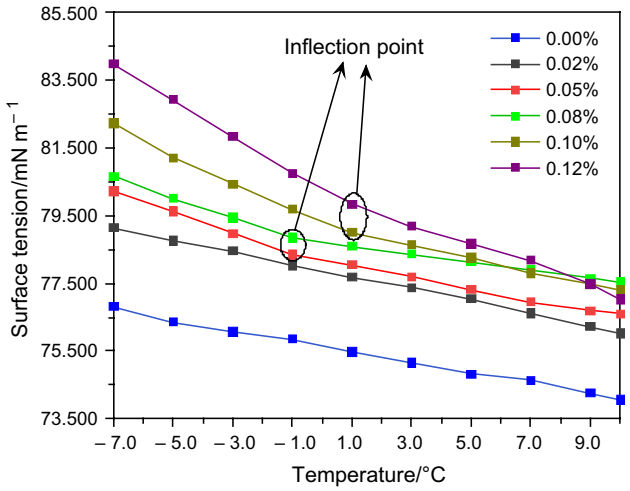

Fig. 10 Surface tension of graphene oxide nanofluid varies with temperature

tension slowly increases from 79.144 to 80.664 mN m^{-1} when the mass concentration increases from 0.02 to 0.08%. This is likely because the distance between nanoparticles is much larger than the nanoparticle size for such dilute suspensions, so the interactions between nanoparticles have little impact on the surface energy. However, as the mass concentration increases, nanoparticles move closer to each other. Thus, the van der Waals forces increase significantly, which will increase the free energy at the surface and thereby increase surface tension.

Effect of temperature on surface tension

Figure 10 depicts the variation in the surface tension of graphene oxide nanofluids with five mass concentrations and deionized water at different temperatures, and Table 3 shows the corresponding specific data. As seen in Fig. 10 and Table 3, the surface tension of the graphene oxide nanofluids decreases with an increase in temperature. It is consistent with the change trend that the surface tension of all the prepared nanofluids decreases with the raise of temperature whatever the base fluid used [41]. For nanofluids with mass concentrations of 0.02%, the surface tension is 76.000 mN m^{-1} at 10.0 °C and 79.144 mN m^{-1} at − 7.0 °C. When the temperature increases by 17.0 °C, the surface tension decreases by 4.13%. When the temperature increases from − 7.0 to 10.0 °C, the surface tension of nanofluids with mass concentrations of 0.05%, 0.08%, 0.10%, and 0.12% decreases by 4.73%, 4.04%, 6.37%, and 9.04%, respectively. This shows that changes in the surface tension of nanofluids with temperature are affected by the nanofluid's mass concentrations. With an increase in mass concentrations, the change range of surface tension decreases when the increase in temperature is intensified. This may relate to the Brownian motion of nanoparticles [42]. On the one hand, with an increase in temperature, the Brownian movement of the nanoparticles is enhanced, which reduces the concentration

Table 3 Surface tension of graphene oxide nanofluids at different temperatures (unit: mN m^{-1})

Temperature/°C	Graphene oxide nanofluid/mass%					
	0.00	0.02	0.05	0.08	0.10	0.12
− 7.0	76.808	79.144	80.224	80.664	82.228	83.986
− 5.0	76.358	78.761	79.622	80.017	81.203	82.940
− 3.0	76.068	78.447	78.967	79.437	80.429	81.843
− 1.0	75.859	78.033	78.343	78.843	79.695	80.747
1.0	75.476	77.676	78.035	78.592	78.994	79.837
3.0	75.148	77.369	77.700	78.356	78.638	79.194
5.0	74.810	77.043	77.320	78.128	78.256	78.668
7.0	74.629	76.608	76.955	77.898	77.804	78.183
9.0	74.259	76.214	76.694	77.645	77.468	77.487
10.0	74.051	76.000	76.600	77.530	77.300	77.020

Table 4 The change rate of the surface tension of graphene oxide nanofluids with temperature

Graphene oxide nanofluids/mass%	The change rate of surface tension with temperature in non-supercooled state	The change rate of surface tension with temperature in supercooled state
0.00	−0.158	−0.158
0.02	−0.186	−0.185
0.05	−0.159	−0.313
0.08	−0.118	−0.303
0.10	−0.188	−0.422
0.12	−0.313	−0.539

of nanoparticles in the interior of the droplets, weakens the attraction of water molecules at the interface of the droplets, and leads to a decrease in surface tension. On the other hand, a relative increase in the concentration of nanoparticles in a gas/liquid state would enhance the attraction to water molecules and cause the surface tension to increase. Under the influence of these two factors, the surface tension decreases with an increase in temperature.

Meanwhile, the experimental results clearly show that the change rate of surface tension with temperature is different in both a supercooled and non-supercooled state. Data for the change rate of the surface tension with temperature are shown in Table 4.

The value of 0.02 mass% graphene oxide nanofluids and deionized water in supercooled state shows a slight difference from that in non-supercooled state and presents an approximately straight line. However, for a higher mass concentration, the change rate of surface tension with temperature in supercooled state is obviously greater than that in non-supercooled state. Further, there is an inflection point in the surface tension curve, for nanofluids with mass concentrations of 0.05% and 0.08%, the inflection point is at −1.0 °C, while for mass concentrations of 0.10% and 0.12%, the inflection point is at 1.0 °C, and the inflection point is close to the triple point temperature of water, and it may be related to the addition of graphene oxide nanomaterial. Similar phenomena have been reported in some previous studies [43–45]. In addition, under a supercooled state, the change rate of the surface tension increases with an increase in mass concentration. This result is likely related to the distribution of nanoparticles in supercooled state. Moreover, the surface tension of the supercooled and non-supercooled states shows a linear change trend.

Conclusions

The surface tension measurements of graphene oxide nanofluids with mass concentrations of 0.02%, 0.05%, 0.08%, 0.10%, and 0.12% were taken using an acoustic levitator. The surface tension data for the graphene oxide nanofluids in supercooled state are thus enriched. Containerless processing and noncontact measurement techniques eliminated contamination from the container wall, which enabled the accurate measurement of fluid in supercooled state. In both supercooled and non-supercooled states, the surface tension of nanofluids increased with an increase in mass concentration at the same temperature and decreased with an increase in temperature. When the mass concentration is lower than 0.08%, the surface tension continues to increase slowly with the increase in the mass concentration. The change rate with temperature of the surface tension of 0.02 mass% graphene oxide nanofluids in supercooled state is basically the same as that in non-supercooled state and presents an approximately straight line. However, for higher mass concentrations of nanofluids, the change rate of the surface tension with temperature in supercooled state is obviously different from that in non-supercooled state, and there is an inflection point near the triple point temperature of the water. Moreover, the surface tension of nanofluids in both supercooled and non-supercooled states shows a linear variation trend.

Acknowledgements The authors gratefully acknowledge the financial support provided by the technology innovation and application development special project of Chongqing, China (Grant Number: cstc2019jscx-msxmX0046).

References

1. Choi SUS, Eastman JA. Enhancing thermal conductivity of fluids with nanoparticles. Lemont: Argonne National Lab; 1995.
2. Gomez-Villarejo R, Aguilar T, Hamze S, et al. Experimental analysis of water-based nanofluids using boron nitride nanotubes with improved thermal properties. J Mol Liq. 2019;277:93–103. https://doi.org/10.1016/j.molliq.2018.12.093.
3. Selvaraj V, Morri B, Nair LM, et al. Experimental investigation on the thermophysical properties of beryllium oxide-based nanofluid and nano-enhanced phase change material. J Therm Anal Calorim. 2019;137(5):1527–36. https://doi.org/10.1007/s10973-019-08042-w.
4. Gomez-Villarejo R, Estellé P, Navas J. Boron nitride nanotubes-based nanofluids with enhanced thermal properties for use as heat transfer fluids in solar thermal applications. Sol Energy Mater Sol Cells. 2020;205:110266. https://doi.org/10.1016/j.solmat.2019.110266.
5. Fares M, Al-Mayyahi M, Al-Saad M. Heat transfer analysis of a shell and tube heat exchanger operated with graphene

nanofluids. Case Stud Therm Eng. 2020;18:100584. https://doi.org/10.1016/j.csite.2020.100584.
6. Yudong L, Jiangqing W, Chuangjian S, et al. Nucleation rate and supercooling degree of water-based graphene oxide nanofluids. Appl Therm Eng. 2017;115:1226–36. https://doi.org/10.1016/j.applthermaleng.2016.10.051.
7. Sidik NAC, Kean TH, Chow HK, et al. Performance enhancement of cold thermal energy storage system using nanofluid phase change materials: a review. Int Commun Heat Mass Transf. 2018;94:85–95. https://doi.org/10.1016/j.icheatmasstransfer.2018.03.024.
8. Jing F, Yixin L, Pengjv M, et al. Supercooling and heterogeneous nucleation in acoustically levitated deionized water and graphene oxide nanofluids droplets. Exp Therm Fluid Sci. 2019;103:143–8. https://doi.org/10.1016/j.expthermflusci.2019.01.016.
9. Guo Z, Haynes BS, Fletcher DF. Simulation of microchannel flows using a 3D height function formulation for surface tension modelling. Int Commun Heat Mass Transf. 2017;89:122–33. https://doi.org/10.1016/j.icheatmasstransfer.2017.09.017.
10. Kováts P, Thévenin D, Zähringer K. Influence of viscosity and surface tension on bubble dynamics and mass transfer in a model bubble column. Int J Multiph Flow. 2020;123:103174. https://doi.org/10.1016/j.ijmultiphaseflow.2019.103174.
11. Ferri JK, Carl P, Gorevski N, et al. Separating membrane and surface tension contributions in Pickering droplet deformation. Soft Matter. 2008;4(11):2259–66. https://doi.org/10.1039/B805088K.
12. Croce R, Griebel M, Schweitzer MA. Numerical simulation of bubble and droplet deformation by a level set approach with surface tension in three dimensions. Int J Numer Methods Fluids. 2010;62(9):963–93. https://doi.org/10.1002/fld.2051.
13. Ding SY, Wang RX, Xu RJ, et al. Effect of surface tension on deformation of free falling drops. Ciesc J. 2016;67(6):2495–502. https://doi.org/10.11949/j.issn.0438-1157.20151867.
14. Wan Q, Zhao J, Li H, et al. The wetting behavior of three different types of aqueous surfactant solutions on housefly (*Musca domestica*) surfaces. Pest Manag Sci. 2019;76(3):1085–93. https://doi.org/10.1002/ps.5620.
15. Premnath KN, Hajabdollahi F, Welch SW. Surfactant effects on interfacial flow and thermal transport processes during phase change in film boiling. Phys Fluids. 2018;30(4):042108. https://doi.org/10.1063/1.5010333.
16. Song D, Song B, Hu H, et al. Effect of a surface tension gradient on the slip flow along a superhydrophobic air–water interface. Phys Rev Fluids. 2018;3(3):033303. https://doi.org/10.1103/PhysRevFluids.3.033303.
17. Zheng ZZ. Experimental investigation on surface tension of water-based graphene oxide nanofluids. J Therm Sci Technol. 2015;14(3):203–7. https://doi.org/10.1016/10.13738/j.issn.1671-8097.2015.03.006.
18. Kamatchi R, Venkatachalapathy S, Srinivas BA. Synthesis, stability, transport properties, and surface wettability of reduced graphene oxide/water nanofluids. Int J Therm Sci. 2015;97:17–25. https://doi.org/10.1016/j.ijthermalsci.2015.06.011.
19. Ahammed N, Asirvatham LG, Wongwises S. Effect of volume concentration and temperature on viscosity and surface tension of graphene–water nanofluid for heat transfer applications. J Therm Anal Calorim. 2016;123(3):1399–409. https://doi.org/10.1007/s10973-015-5034-x.
20. Cabaleiro D, Estellé P, Navas H. Dynamic viscosity and surface tension of stable graphene oxide and reduced graphene oxide aqueous nanofluids. J Nanofluids. 2018;7(6):1081–8. https://doi.org/10.1166/jon.2018.1539.
21. Tanvir S, Qiao L. Surface tension of nanofluid-type fuels containing suspended nanomaterials. Nanoscale Res Lett. 2012;7(1):1–10. https://doi.org/10.1186/1556-276X-7-226.
22. Karthikeyan A, Coulombe S, Kietzig AM. Wetting behavior of multi-walled carbon nanotube nanofluids. Nanotechnology. 2017;28(10):1. https://doi.org/10.1088/1361-6528/aa5a5f.
23. Berrada N, Hamze S, Desforges A. Surface tension of functionalized MWCNT-based nanofluids in water and commercial propylene-glycol mixture. J Mol Liq. 2019. https://doi.org/10.1016/j.molliq.2019.111473.
24. Karami H, Papari-Zare S, Shanbedi M, et al. The thermophysical properties and the stability of nanofluids containing carboxyl-functionalized graphene nano-platelets and multi-walled carbon nanotubes. Int Commun Heat Mass Transf. 2019;108:104302. https://doi.org/10.1016/j.icheatmasstransfer.2019.104302.
25. Geng D, Xie WJ, Hong ZY. Containerless solidification of Ag–Cu eutectic alloy under acoustic levitation condition. Sci Sin Physica Mech Astron. 2011;41(3):227. https://doi.org/10.1360/132010-975.
26. Bouyer C, Chen P, Güven S, et al. A bio-acoustic levitational (BAL) assembly method for engineering of multilayered, 3D brain-like constructs, using human embryonic stem cell derived neuro-progenitors. Adv Mater. 2016;28(1):161–7. https://doi.org/10.1002/adma.201503916.
27. Hirayama R, Plasencia DM, Masuda N, et al. A volumetric display for visual, tactile and audio presentation using acoustic trapping. Nature. 2019;575(7782):320–3. https://doi.org/10.1038/s41586-019-1739-5.
28. Okada JT, Ishikawa T, Watanabe Y, et al. Surface tension and viscosity of molten vanadium measured with an electrostatic levitation furnace. J Chem Thermodyn. 2010;42(7):856–9. https://doi.org/10.1016/j.jct.2010.02.008.
29. Zang D, Yu Y, Chen Z, et al. Acoustic levitation of liquid drops: dynamics, manipulation and phase transitions. Adv Colloid Interface Sci. 2017;243:77–85. https://doi.org/10.1016/j.cis.2017.03.003.
30. Hasegawa K, Watanabe A, Kaneko A, et al. Coalescence dynamics of acoustically levitated droplets. Micromachines. 2020;11(4):343. https://doi.org/10.3390/mi11040343.
31. Lv YJ. Drop dynamics and solidification mechanism of water and aqueous solution under acoustic levitation. Xian: Northwestern Polytechnical University; 2009.
32. Mehrali M, Sadeghinezhad E, Latibari ST, et al. Investigation of thermal conductivity and rheological properties of nanofluids containing graphene nanoplatelets. Nanoscale Res Lett. 2014;9(1):15. https://doi.org/10.1186/1556-276X-9-15.
33. Rayleigh L. On the capillary phenomena of jets. Proc R Soc Lond. 1879;29(196–199):71–97.
34. Soda H, McLean A, Miller WA. The influence of oscillation amplitude on liquid surface tension measurements with levitated metal droplets. Metall Mater Trans B. 1978;9(1):145–7.
35. Shen C, Xie W, Wei B. Digital image processing of sectorial oscillations for acoustically levitated drops and surface tension measurement. Sci China Phys Mech Astron. 2010;53(12):2260–5. https://doi.org/10.1007/s11433-010-4125-8.
36. Zang D, Chen Z, Geng X. Sectorial oscillation of acoustically levitated nanoparticle-coated droplet. Appl Phys Lett. 2016;108(3):031603-1–4. https://doi.org/10.1063/1.4940143.
37. Canny J. A computational approach to edge detection. IEEE Trans Pattern Anal Mach Intell. 1986;6:679–98. https://doi.org/10.1109/TPAMI.1986.4767851.
38. Vargaftik NB, Volkov BN, Voljak LD. International tables of the surface tension of water. J Phys Chem Ref Data. 1983;12(3):817–20. https://doi.org/10.1063/1.555688.
39. Reincke F, Hickey SG, Kegel WK, et al. Spontaneous assembly of a monolayer of charged gold nanocrystals at the water/oil

interface. Angew Chem Int Ed. 2004;43(4):458–62. https://doi.org/10.1002/anie.200352339.
40. Vafaei S, Purkayastha A, Jain A, et al. The effect of nanoparticles on the liquid–gas surface tension of Bi_2Te_3 nanofluids. Nanotechnology. 2009;20(18):185702. https://doi.org/10.1088/0957-4484/20/18/185702.
41. Estelléa P, Cabaleiro D, Żyła G, et al. Current trends in surface tension and wetting behavior of nanofluids. Renew Sustain Energy Rev. 2018;94:931–44. https://doi.org/10.1016/j.rser.2018.07.006.
42. Saada MA, Chikh S, Tadrist L. Evaporation of a sessile drop with pinned or receding contact line on a substrate with different thermophysical properties. Int J Heat Mass Transf. 2013;58(1–2):197–208. https://doi.org/10.1016/j.ijheatmasstransfer.2012.11.026.
43. Lü YJ, Wei B. Second inflection point of water surface tension. Appl Phys Lett. 2006;89(16):164106-1–3. https://doi.org/10.1063/1.2364167.
44. Kalova J, Mares R. Second inflection point of the surface tension of water. Int J Thermophys. 2012;33(6):992–9. https://doi.org/10.1007/s10765-012-1238-5.
45. Wang X, Binder K, Chen C, et al. Second inflection point of water surface tension in the deeply supercooled regime revealed by entropy anomaly and surface structure using molecular dynamics simulations. Phys Chem Chem Phys. 2019;21(6):3360–9. https://doi.org/10.1039/C8CP05997G.

Publisher's Note Springer Nature remains neutral with regard to jurisdictional claims in published maps and institutional affiliations.